DIRECT AND INVERSE METHODS FOR SCATTERING BY CRACKS AT HIGH FREQUENCIES

J. D. Achenbach
The Technological Institute
Northwestern University
Evanston, IL 60201

ABSTRACT

Further results are presented for the direct problem of scattering of high-frequency waves by cracks in elastic solids. Results for a penny-shaped crack, obtained on the basis of geometrical diffraction theory, are compared with experimental data. For simple crack geometries a hybrid method, whereby the crack-opening displacement is computed by ray theory, and the scattered field is subsequently obtained by the use of a representation theorem, is tested by comparison with exact results. The simple form of the far-field high-frequency solutions to the direct scattering problem suggests the application of Fourier-type integrals to solve the inverse problem. Two different inversion integrals are discussed. The inversion method is checked by applying it to the scattered field of a flat elliptical crack, for which an analytical expression is derived. Some computational technicalities are discussed, and numerical results are presented.

INTRODUCTION

Several recent publications have been concerned with solutions to the direct problem of high-frequency scattering of time-harmonic waves by cracks in elastic solids. From the phenomenological point of view the high-frequency approach is appealing in that the probing wavelengths are of the same order of magnitude as the length-dimensions of the crack. This gives rise to interesting and detectable characteristic interference phenomena. The high-frequency approach is also very attractive from the mathematical point of view, because the intuitively straightforward methods of elastodynamic ray theory can be applied to yield accurate solutions.

For flat cracks with a smoothly curved edge in the interior of a homogeneous, isotropic, linearly elastic body, the direct scattering problem in the high-frequency domain can now be solved accurately, provided that ka is sufficiently larger than unity, where k is the wavenumber and a is a characteristic radius of curvature of the crack edge. Results, which have been obtained on the basis of either geometrical diffraction theory (GTD), or a hybrid method, whereby the crack-opening-displacement (COD) is computed on the basis of GTD, and the scattered field is subsequently obtained by the use of a representation theorem, have been reported by Achenbach et al[1,2].

In the present paper a very brief summary of GTD is given, and some recent comparisons with experimental results are reviewed. For simple crack geometries, the hybrid method is tested by comparisons of both COD computations and scattered-field computations with exact results which have been obtained by numerical solution of a governing singular integral equation.

A major part of the present paper is devoted to the inverse problem. It is known that at high frequencies the far-field generated by a volume scatterer in an acoustic medium is proportional to the Fourier transform of the characteristic function associated with the scatterer. The characteristic function is defined so that it has unit value for every point inside the scatterer and vanishes elsewhere. The Fourier transform parameter which enters in this relation is a function of the wave-number and the angle of observation. A number of studies have recently been devoted to examine the extent to which the far-field data can be used to numerically invert this Fourier transform relation and recover the size, shape and the location of the scatterer. In these studies the possible limitation on the bandwidths of the observed scattered signals has been taken into account, as well as the restricted range of the aperture covered by the angles of observation. For details, the reader is referred to the recent work of Cohen and Bleistein[3,4].

In the present paper the inversion of far-field crack-scattering data in the high-frequency range by a method which does not involve a three dimensional Fourier inversion but only a single integration in the wave-number domain is discussed. The method was introduced by Achenbach et al[5], and it is further explored in the present paper.

ELASTODYNAMIC RAY THEORY

Ray theory provides a method to trace the amplitude of a high-frequency disturbance as it propagates along a ray. In a homogeneous, isotropic, linearly elastic solid the rays are straight lines, which are normal to the wavefronts. An unbounded solid can support rays of longitudinal and transverse wave motion. These rays are denoted as L-rays and T-rays, respectively.

In analogy with geometrical optics, the simplest theory for diffraction of elastic waves by cracks may be called geometrical elastodynamics (GE). In GE a crack acts as a screen which creates a shadow zone of no motion, and zones of reflected waves. The geometrical theory of diffraction (GTD) provides a first correction to GE, in that terms arising from edge diffraction are

taken into account.

For plane longitudinal and transverse waves, which are under arbitrary angles of incidence with a traction-free semi-infinite crack, the fields on the diffracted rays can be obtained by asymptotic considerations, as shown by Achenbach et al[6,7]. The results can be expressed in terms of diffraction coefficients which relate the diffracted fields to the incident fields. Geometrical diffraction theory provides modifications to the semi-infinite crack results, to account for curvature of incident wave-fronts and curvature of crack edges, and finite dimensions of the crack. In the usual terminology the results for diffraction of plane waves by a semi-infinite crack are the canonical solutions. For incident waves with curved wavefronts and for curved diffracting edges, the cones of diffracted rays have envelopes, at which the rays coalesce and the fields become singular. The envelopes are called caustics, and GTD breaks down at caustics.

A more complete discussion of GTD can be found in the papers by Achenbach et al[1,2].

Experiment. Experimental results in the high-frequency range that are suitable for comparison with theoretical results have been reported by Adler et al[8,9]. The sample was a circular disk (2.5 x 10 cm) of titanium alloy which contained a penny-shaped crack of radius 2500μ parallel to the flat faces, and located at the center of the disk. The disk was immersed in water. A transmitter launched a longitudinal wave to the water-titanium interface under normal incidence. This wave was transmitted into the solid, diffracted by the crack, and the diffracted waves were transmitted back into the fluid, where they were received by a second transducer. The experimental set-up and the processing of the data are discussed in some detail elsewhere[9].

In the experimental work the nature of the diffracted signals is determined by their arrival times. Since the first arriving signals are related to longitudinal waves in the solid, it is possible to gate out and separate the purely longitudinal diffracted signals from subsequent signals. By appropriate processing of the experimental data, as discussed in Ref. 9, the amplitude-spectrum is obtained for the longitudinal diffracted waves only. Thus for the present comparison of analytical and experimental results we need to consider only the primary diffracted body-wave rays in our analytical work.

The interference patterns for the first arriving longitudinal waves in the fluid are generated by phase differences and amplitude differences on the direct rays from the two crack tips, see Fig. 1. Adding the primary diffracted longitudinal fields from the points 0_1 and 0_2 we obtain in the far-field

$$u_L \sim F(\theta,\theta_0)\exp\left[i\omega(S/c_L + \bar{S}/c_F) + i\pi/4\right] U_0 \underset{\sim}{i}_F \quad (1)$$

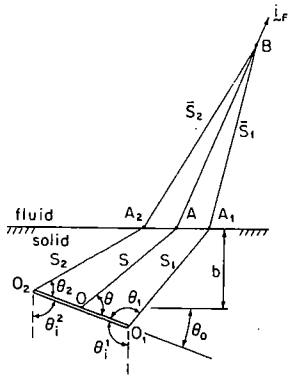

Fig. 1: Geometry in the plane of symmetry of a penny-shaped crack.

$$F(\theta,\theta_0) = H_1\exp\left[-i(\omega a/c_L)(\cos\theta - \sin\theta_0)\right] + H_2\exp\left[i(\omega a/c_L)(\cos\theta - \sin\theta_0)\right] \quad (2)$$

$$H_j = \frac{\operatorname{sgn}(\cos\theta_j)\, T(\theta_L^j)\, |D_L^L(\theta_j;\theta_i^j)|}{(\omega S_j/c_L)^{1/2}(1+S_j/C)^{1/2}(1+\bar{S}_j/\bar{E})^{1/2}(1+\bar{S}_j/\bar{C})^{1/2}}$$

$$j = 1,2 \quad (3)$$

Here ω is the circular frequency, a is the crack radius, $\bar{S} = \overline{AB}$, U_0 represents the incident wave at point 0, and c_L and c_F are the velocities of longitudinal waves in solid and fluid respectively. The geometrical quantities are indicated in Fig. 1. In Eq.(3) T(.) is the transmission coefficient at the solid-fluid interface, and $D_L^L(\cdot;\cdot)$ is the diffraction coefficient. For details of the derivation of Eqs.(1) - (3) we refer to Ref. 9. It should be noted that one of the terms H_j is imaginary, since the ray has crossed a caustic. Of particular interest is the absolute magnitude of F,

$$|F| = \{\,|H_1|^2 + |H_2|^2 + 2|H_1||H_2|\sin 2(\omega a/c_L)(\cos\theta - \sin\theta_0)\,\}^{1/2} \quad (4)$$

Here we have taken into account that either H_1 or H_2 is imaginary.

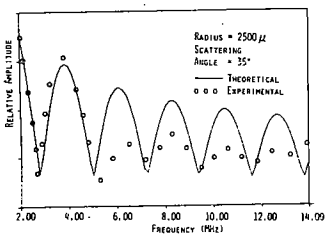

Fig. 2: Comparison of Eq. (4) with experimental results in Ref. 9.

Comparisons with Experimental Data. Theoretical results obtained from Eq.(4) have been plotted together with experimental data in Fig. 2. The frequency varies from 2 MHz to about 14 MHz. The angle in the solid is $\theta'(=\pi/2 - \theta) = 35^{o}$ respectively. The amplitudes of the first few cycles agree well. At higher frequencies (above 6 MHz) the experimental results are lower than predicted by theory. One possible explanation is the effect of attenuation which is not accounted for in the theory. In all cases the positions of maxima and minima of the spectra agree well. The locations of the maxima are significant for the inversion process. Additional comparisons with experimental data have been reported in Ref. 9.

A HYBRID METHOD

In this method the crack-opening-displacement (COD) is computed on the basis of elastodynamic ray theory, and the diffracted field is subsequently obtained by the use of a representation theorem. The advantage of this approach is that the trouble with ray theory at shadow boundaries and boundaries of zones of specular reflection is eliminated, and caustics only need to be dealt with on the faces of the crack.

Elastodynamic representation theorem. The field generated by scattering of incident waves by an obstacle with surface S can be expressed in terms of a representation integral over S. For a stress-free crack with plane faces A^+ and A^- the representation integral can be simplified. If the total field is written as $\underline{u}^t = \underline{u}^{in} + \underline{u}^{sc}$, where $\underline{u}^{in}$ is the incident field and $\underline{u}^{sc}$ is the scattered field, then at an arbitrary field point $\underline{x}$ the latter can be expressed in the form

$$u_m^{sc}(\underline{x}) = \int_{A^+} \tau^G_{ij;m}(\underline{x}-\underline{X})\Delta u_i^{sc}(\underline{X})\, n_j\, dA(\underline{X}) \qquad (5)$$

Here $\underline{x}$ represents any point outside of the crack, and $\underline{n}$ is the outward normal (pointing from the A^+ to the A^- face). Also $\Delta u_i(\underline{X})$ is the crack-opening displacement defined by

$$\Delta u_i^{sc}(\underline{X}) = (u_i^{sc})_{A^+} - (u_i^{sc})_{A^-} \qquad (6)$$

and

$$\tau^G_{ij;m} = \text{tensor of rank three}, \qquad (7)$$

which represents the stress-components at $\underline{X}$ due to a unit load in the x_m direction at the point defined by $\underline{X}$. Provided that the crack-opening-displacement can be adequately approximated, Eq.(5) may be expected to give a good approximation to the scattered field. In this section we employ GTD to compute an approximation to the COD.

Crack-opening displacement. Four principal difficulties must be overcome, in the hybrid method presented here. First, GTD predicts unbounded COD's at the crack edge. It is however, seen below by comparison with exact numerical results that this effect is negligible. Secondly, caustics remain, although they are reduced by one dimension. In GTD caustic surfaces occur. To compute the COD, only caustic curves which are confined to the crack faces are encountered. Thirdly, Eq.(5) must be numerically integrated which becomes progressively more difficult with decreasing wave lengths. Finally, the computation of the COD becomes more complicated if "boundary-waves" are included to achieve the desired accuracy.

We now give a brief description of the terms included in the COD, with emphasis on the boundary-wave terms. The COD can be represented by

$$\Delta u_j = \Delta u_j^{GE} + \Delta u_j^{S} + \Delta u_j^{TH} + \Delta u_j^{BL} + \Delta u_j^{BT} \qquad (8)$$

The first term is the geometrical elastodynamics (GE) contribution to the COD. On the illuminated crack face it consists of the incident wave and the specular reflections. The GE contribution vanishes on the crack face at the shadow side. The second term consists of the diffracted and reflected surface waves which have been described in the previous section. This term is of order one in wavelength with respect to the incident wave. The third term is the contribution to the COD from the diffracted body waves. It includes only horizontally polarized transverse rays, and it is of order the square root in wavelength with respect to the incident wave. We note that the longitudinal diffraction coefficients and those parts of the transverse diffraction coefficients which give rise to vertically polarized waves vanish on the crack faces. The last two terms are the boundary-wave contributions to the COD. In principle they are of order three halves power in wavelength with respect to the incident wave. However, at moderate wave numbers, their amplitude can be large.

Boundary-waves occur because the diffracted body waves do not satisfy the boundary conditions of vanishing traction on the crack faces. The transverse boundary-wave (which is generally known as the "head-wave") and the diffracted longitudinal body-wave combine to satisfy the boundary condition of vanishing tangential tractions on the crack faces. The longitudinal boundary-wave and the diffracted transverse body-wave combine to satisfy the boundary condition of vanishing normal tractions on the crack faces. More details can be found in a paper by Gautesen [10]. From the mathematical point of view, boundary-waves represent branch-point contributions to the inverse Fourier transforms of the displacement fields. The amplitude of the longitudinal boundary-wave is large at moderate wave numbers due to the proximity of the Rayleigh pole to the branch point. The amplitude of the transverse boundary-wave is large at moderate wave numbers because the branch point is close to the extraneous roots of the rationalized Rayleigh function.

SOME RESULTS

In this section we present comparisons between the scattered fields computed by GTD, by the hybrid method and by exact theory, for a penny-shaped crack and for a slit.

For the penny-shaped crack we consider normal incidence of a longitudinal wave. The radius of the crack is a, and the origin of an (r,θ)-coordinate system is placed at the center of the crack, where r and θ vary in a plane normal to the plane of the crack. Thus $\theta = 0$ in the plane of the crack, and $\theta = \pi/2$ along a line through the center of the crack normal to the crack-plane.

A dimensionless crack-opening displacement computed by the method discussed in the previous section is shown in Fig. 3. It is noted that the agreement between the exact COD (solid line) and the approximate COD (dashed line) is excellent. The approximate COD, which is relatively easy to obtain can be substituted in Eq.(5) to obtain the scattered field.

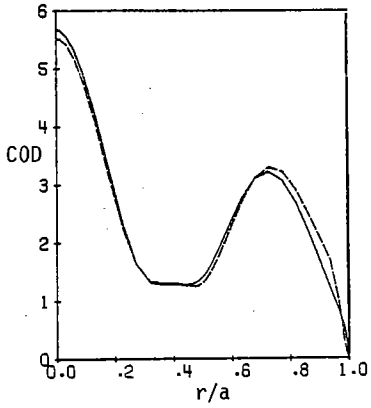

Fig. 3 Dimensionless crack-opening displacement for normal incidence of a longitudinal wave on a penny-shaped crack; $\nu = 0.25$, $k_L a = 5$; —— exact theory, - - - approximate COD.

Comparisons of the scattered displacements as functions of the angle θ, for $r/a = 10$ and $k_L a = 5$ are shown in Figs. 4 and 5. The GTD results have been corrected at the shadow boundary and at the line through the center of the crack normal to the crack-plane (which is a caustic). For the scattered displacement in the x_2-direction (normal to the crack) there are, however, still deviations near the shadow boundary.

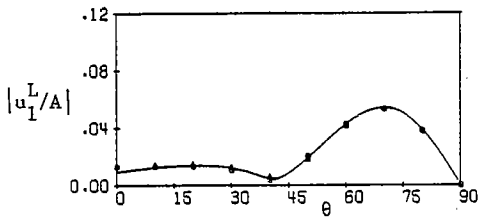

Fig. 4 Scattered longitudinal x_1-displacement for normal incidence of a longitudinal wave; $r/a = 10$, $k_L a = 5$; —— GTD, ▲ hybrid theory, o exact results.

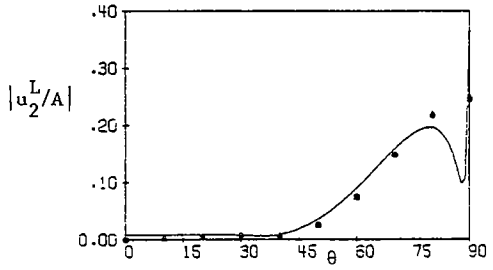

Fig. 5 Scattered longitudinal x_2-displacement for normal incidence of a longitudinal wave; $r/a = 10$, $k_L a = 5$; —— GTD, ▲ hybrid theory, o exact results.

Figure 6 shows the geometry of a slit with oblique incidence of a longitudinal wave. Comparisons of the displacements are shown in Fig. 7. The agreement is generally better for the scattered longitudinal-wave displacements than for the scattered transverse-wave displacements.

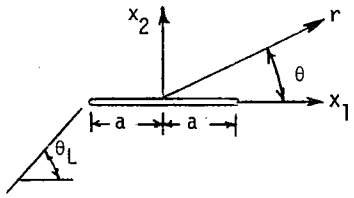

Fig. 6 2-D Geometry for a slit

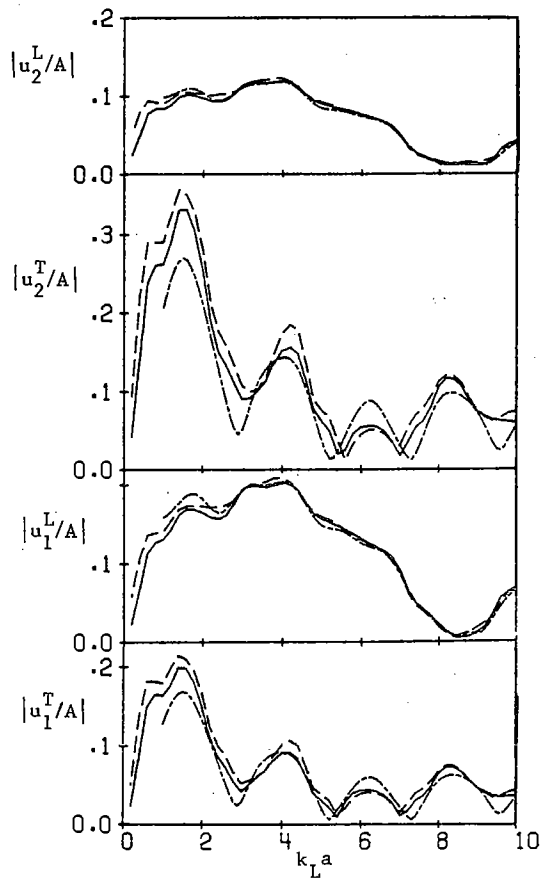

Fig. 7 Displacements due to scattered waves versus $k_L a$; $r/a = 10$, $\nu = 0.25$, angle of incidence $\theta_L = 60^o$; —— exact, - - - hybrid method, —·— GTD, $\theta = 30^o$.

The far-field longitudinal solution. Let us assume that the origin 0 of the coordinate system is close to the crack while the source S of the incident field and the observation point Q are far away, see Fig.8

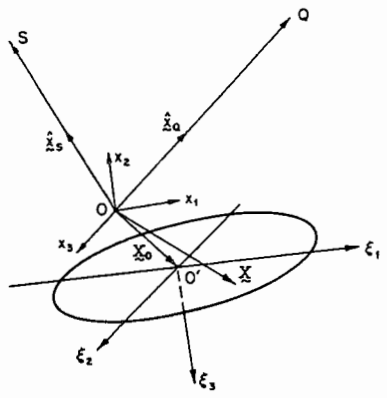

Fig. 8 Flat crack, with source point S and point of observation Q.

Thus, if $\underline{x}_S$, $\underline{x}_Q$, and $\underline{X}$ denote the position vectors of S, Q and any point on the crack, and $x_S = |\underline{x}_S|$, $x_Q = |\underline{x}_Q|$ and $X = |\underline{X}|$, then x_S, $x_Q >> X$. Defining the unit vector $\hat{x}_Q = \underline{x}_Q/x_Q$, we can write

$$|\underline{x}_Q - \underline{X}| \sim x_Q - (\hat{x}_Q \cdot \underline{X}), \quad x_Q >> X \tag{9}$$

The expression for $\tau^G_{ij;m}$ then simplifies considerably. Substituting this simplified result in Eq. (5), we find for the longitudinal field

$$\{u^{sc}_m(\underline{x}_Q)\}^L = -ik_L b^{G;L}_{ij;m}(\hat{x}_Q) G_L(x_Q) n_j I^L_i(\hat{x}_Q) \tag{10}$$

where

$$b^{G;L}_{ij;m} = (\lambda + 2\mu)^{-1} (2\mu\, \hat{x}_i \hat{x}_j + \lambda\, \delta_{ij})\, \hat{x}_m \tag{11}$$

$$G_L(x) = \frac{1}{4\pi x} \exp(ik_L x) \tag{12}$$

$$k_L = \omega/c_L \;; \quad c_L^2 = (\lambda + 2\mu)/\rho \tag{13}$$

and

$$I^L_i(\hat{x}_Q) = \int_{A^+} \exp(-ik_L \underline{x}_Q \cdot \underline{X}) \Delta u^{sc}_i(\underline{X})\, dA(\underline{X}) \tag{14}$$

In Eq. (10) the summation convention applies, and in (11)-(13) λ and μ are Lamé's elastic constants, and ρ is the mass density.

PHYSICAL ELASTODYNAMICS

The physical elastodynamics approximation is obtained if only the leading contributions arising from the incident field and the specularly reflected body waves from the illuminated face are included in $\Delta\underline{u}$, i.e.,

$$\Delta\underline{u}^{sc} \sim \Delta\underline{u}^{GE} = -(\underline{u}^{in} + \underline{u}^{re})^{A^-} \tag{15}$$

For the incident field we assume a longitudinal wave from S given by

$$\underline{u}^{in} = -A\, \hat{\underline{x}}_S\, G_L(x_S) \exp(-ik_L \hat{\underline{x}}_S \cdot \underline{X}) \;, \quad x_S >> X \tag{16}$$

The reflected field $\underline{u}^{re}$ from A^- can be found from the standard results on reflection of plane waves, as

$$\Delta\underline{u}^{sc} \sim A\, \underline{\alpha}(\hat{\underline{x}}_S)\, G_L(x_S) \exp(-ik_L \hat{\underline{x}}_S \cdot \underline{X}) \tag{17}$$

An expression for $\underline{\alpha}(\hat{\underline{x}}_S)$ can be found elsewhere.[5] Substitution of (17) into (14) yields the scattered longitudinal far-field as

$$\frac{\{u^{sc}_m(\underline{x}_Q)\}^L}{G_L(x_S) G_L(x_Q)} = -A\, \alpha_i(\hat{\underline{x}}_S) b^{G;L}_{ij;m}(\hat{\underline{x}}_Q) n_j\, I(k_L) \tag{18}$$

where

$$I(k_L) = ik_L \int_{A^+} \exp(-ik_L \underline{q} \cdot \underline{X})\, dA(\underline{X}) \tag{19}$$

and

$$\underline{q} = (\hat{\underline{x}}_S + \hat{\underline{x}}_Q) \tag{20}$$

is a vector in the bisector-direction of $\overline{OS}$ and $\overline{OQ}$. The far-field dependence on the crack occurs only through the function $I(k_L)$, which depends on the wave-number k_L and the bisector-vector $\underline{q}$.

Various alternate expressions can be written for the integral $I(k_L)$. After introducing the ξ_1 and ξ_2 coordinates in the plane of the crack, see Fig. 8 , $I(k_L)$ can be reduced to

$$I(k_L) = -\frac{\exp(-ik_L \underline{q} \cdot \underline{X})}{q_1^2 + q_2^2} \int_C \underline{\nu} \cdot \underline{q} \exp(-ik_L \underline{q} \cdot \underline{\xi})\, ds \tag{21}$$

where $\underline{\nu}$ is the outward unit normal to the crack edge, and s is arc length measured along the crack edge C. By means of Eq. (21) the scattered longitudinal field is expressed as radiation generated by a superposition of sources over the edge of the crack. This kind of representation seems to be analogous to the method of equivalent currents, which has been explored by several authors in electromagnetic scattering theory.

It is convenient to consider still another system defined by (see Fig. 9)

$$\bar{\xi}_1 = q_1 \xi_1 + q_2 \xi_2 \;; \quad \bar{\xi}_2 = -q_2 \xi_1 + q_1 \xi_2 \;;$$

$$\bar{\xi}_3 = \xi_3 \tag{22}$$

Note that the $\bar{\xi}_1$-axis is parallel to the projection

of $\underline{q}$ on the crack-plane. The q_i used here are defined in the $\underline{\xi}$-system. Then Eq. (18) can be reduced to the simple form[5]

$$I(k_L) = -\frac{\exp(-ik_L \underline{q}\cdot\underline{X}_o)}{q_1^2 + q_2^2} \int_C \exp(-ik_L \bar{\xi}_1)\, d\bar{\xi}_2 \quad (23)$$

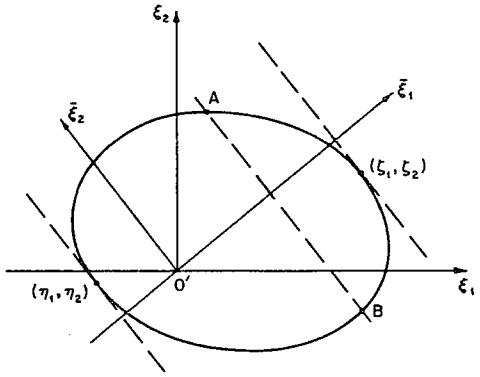

Fig. 9 Coordinates in the plane of the crack

Another useful approximation results by introducing local coordinates near the points E and F on C where the tangents are parallel to the $\bar{\xi}_2$-axis, (see Fig. 9). For instance, near $E(\zeta_1,\zeta_2,0)$, the points on C can be represented by

$$\bar{\xi}_1 = \zeta_1 + \frac{1}{2!} s^2 \beta_o + \frac{1}{3!} s^3 \beta_1 \quad (24)$$

$$\bar{\xi}_2 = \zeta_2 + s - \frac{1}{3!} s^3 \beta_o^2 \quad (25)$$

where s is measured from $E(\zeta_1,\zeta_2,0)$ and β_o and β_1 are the curvature of C and the value of $d\beta_o/ds$ at this point. We next substitute (24) and (25) into Eq. (23) and apply the stationary-phase approximation. The contribution from $E(\zeta_1,\zeta_2,0)$ then becomes

$$I(k_L) \sim -\frac{(2\pi)^{\frac{1}{2}} e^{-i\pi/4}}{(q_1^2 + q_2^2)\beta_o^{\frac{1}{2}}} k_L^{-\frac{1}{2}} \exp\{-ik_L(\zeta_1 + \underline{q}\cdot\underline{X}_o\} \quad (26)$$

where

$$\zeta_1 = (a^2 q_1^2 + b^2 q_2^2)^{\frac{1}{2}} \quad (27)$$

A similar contribution arises also from $F(\eta_1,\eta_2,0)$. Details of the derivation of Eqs. (21), (23) and (26) can be found in Ref. 5.

It is of interest to note that for a crack of elliptical shape defined by

$$\xi_1^2/a^2 + \xi_2^2/b^2 = 1 \; ; \; \xi_3 = 0 \quad (28)$$

Eq. (21) can be evaluated analytically to give

$$I(k_L) = -2\pi i \frac{ab}{\rho} J_1(k_L\zeta_1) \exp(-ik_L \underline{q}\cdot\underline{X}_o) \quad (29)$$

where $J_1(\;)$ is the cylindrical Bessel function, and ζ_1 is defined by Eq. (27). The simple result given by (29) in conjunction with (18) has been shown to give quite good agreement with experimental results.[11] It has also proven to be very useful in practical inversion procedures based on the application of adaptive learning networks.[12]

An asymptotic expression for the Bessel function $J_1(k_L\zeta_1)$ for $k_L\zeta_1 >> 1$ may be written as

$$J_1(k_L\zeta_1) \sim -\frac{1}{2}\left(\frac{2}{\pi k_L \zeta_1}\right)^{\frac{1}{2}} \{\exp[-i(k_L\zeta_1 - 3\pi/4)] + \exp[i(k_L\zeta_1 - 3\pi/4)]\} \quad (30)$$

and it may be checked that the first term in (30) corresponds to the contribution from E stated by (26), while the second term corresponds to the contribution from F.

INVERSION INTEGRALS

The different forms of $I(k_L)$ in Eqs. (21), (23) and (26) suggest simple Fourier-type inversion integrals to recover the size, shape and orientation of a crack from the far-field data. The following inversion integrals have been investigated in some detail in Ref. 5.

$$1.\quad f_1^*(\underline{\lambda}) = \int_{-\infty}^{\infty} \exp(ik_L \underline{q}\cdot\underline{\lambda}) f(k_L)\, dk_L \quad (31)$$

$$2.\quad f_2^*(\underline{\lambda}) = \int_{-\infty}^{\infty} k_L^{\frac{1}{2}} \exp(ik_L \underline{q}\cdot\underline{\lambda}) f(k_L) dk_L \quad (32)$$

where $\underline{\lambda}$ defines any test-point in the medium.

Application of the operator of Eq. (31) to the expression for $I(k_L)$ in Eq. (23) gives

$$I_1^*(\underline{\lambda}) = -\frac{1}{(q_1^2 + q_2^2)} \int_C \delta[\underline{q}\cdot(\underline{\lambda} - \underline{X}_o) - \bar{\xi}_1] \frac{d\bar{\xi}_2}{d\bar{\xi}_1} d\bar{\xi}_1 \quad (33)$$

where we have used the relation

$$\int_{-\infty}^{\infty} e^{ik_L\rho}\, dk_L = 2\pi\, \delta(\rho) \quad (34)$$

Evaluating the integral in Eq. (33) by the sifting property of the δ-function we obtain

$$I_1^*(\underline{\lambda}) = \begin{cases} \dfrac{-1}{(q_1^2 + q_2^2)} \left[\left(\dfrac{d\bar{\xi}_2}{d\bar{\xi}_1}\right)^A + \left(\dfrac{d\bar{\xi}_2}{d\bar{\xi}_1}\right)^B\right]_{\bar{\xi}_1 = \kappa} ; (\eta_1 < \kappa < \zeta_1) & (35) \\ 0\;, \; (\kappa < \eta_1 \; ; \; \kappa > \zeta_1) & (36) \end{cases}$$

where

$$\kappa = \underline{q}\cdot(\underline{\lambda} - \underline{X}_o) \quad (37)$$

Here the range of variation of $\bar{\xi}_1$, on C is given by $\eta_1 < \bar{\xi}_1 < \zeta_1$, where η_1 and ζ_1 were defined earlier

in the context of the local coordinate system. In Eq. (35) A and B are the points at which the plane $\xi_1 = \kappa$ intersects the crack edge C when $\eta_1 < \kappa < \zeta_1$. At the extreme positions $\kappa = \zeta_1$ the gradient terms in Eq. (35) become infinite, usually, in the inverse square-root sense, as will later be illustrated by the example of an elliptical crack.

In practice, we can choose $\underline{\lambda}$ along the $\underline{q}$-direction from 0 and determine the finite layer normal to $\underline{q}$ which contains the crack. The singular behavior of the gradient terms will be the principal test for identification of the end-planes of the layers.

The inverse operator of Eq. (31) when applied to Eq. (29) gives

$$I_1^*(\underline{\lambda}) = \begin{cases} \dfrac{2\pi ab}{\zeta_1^2} \dfrac{\kappa}{(\zeta_1^2 - \kappa^2)^{1/2}}; & |\kappa| < \zeta_1 \qquad (38) \\ 0 \ ; & |\kappa| > \zeta_1 \qquad (39) \end{cases}$$

which clearly exhibits the inverse square root singularity at $\kappa = \pm \zeta_1$, where κ is defined in Eq. (37). Conversely it is not difficult to verify that the planes

$$\kappa = \pm \zeta_1 \qquad (40)$$

touch the ellipse at the following points in the $\underline{\xi}$-system:

$$\left(\pm \frac{q_1 a^2}{\zeta_1} \ , \ \pm \frac{q_2 b^2}{\zeta_1} \ , \ 0\right) \qquad (41)$$

These results verify that the application of the inversion integral of Eq. (31) to the expression for the scattered field of longitudinal motion given by Eq. (29), yields two planes which touch the edge of the crack.

It is often desirable to identify the end planes of the layer by a singularity of the Dirac delta function type. To this end we apply the inverse operator defined by Eq. (32) to the stationary phase approximation of $I(k_L)$ given by Eq. (26). This gives

$$I_2^*(\underline{\lambda}) \sim -\frac{(2\pi)^{3/2} e^{-i\pi/4}}{(q_1^2 + q_2^2)(\beta_o)_E^{1/2}} \delta(\kappa - \zeta_1) - \frac{(2\pi)^{3/2} e^{i\pi/4}}{(q_1^2 + q_2^2)(\beta_o)_F^{1/2}} \delta(\kappa - \eta_1) \qquad (42)$$

These expressions have the desired δ-function behavior across the planes $\kappa = \zeta_1$ and $\kappa = \eta_1$.

NUMERICAL EXAMPLES

Source and receiver in a plane of symmetry of the crack. The inversion procedure simplifies tremendously if it can be assumed a-priori that both the source and the receiver are located in a plane of symmetry of the crack. The inversion procedure then becomes essentially two-dimensional. Numerical examples have been discussed in Refs. [5] and [13]. An iteration procedure which improves the accuracy was discussed in some detail in Ref. [5]. Reference [5] also includes an application of the inversion method to the experimental data of Ref. [9].

The 3-D crack. As a 3-D example we consider an elliptical crack of semi-major and semi-minor axes a and b respectively. Relative to a coordinate system at the center of the crack, the ellips is defined by Eq. (28). The diffracted far-field will be assumed in the form discussed earlier, with $I(k_L)$ given by Eq. (29), in terms of a Bessel function. For any given pair of source and observation points, the inverse operator of Eq. (31) will then lead to a pair of end-planes touching the crack edge as given by Eq. (40). The plane of the crack and segments of the crack-edge will now be constructed by using the far-field diffraction data from two source locations S_k, k = 1,2 and a set of observation points Q_n, n = 1, ---20. For our numerical example the spherical coordinates of S_k (k = 1,2) are taken as (25, π/6, π/2) and (25, π/6, 2π/3).

The points Q_n are taken at $\underline{\xi}^{(n)}$ where

$$\xi_1^{(n)} = 10 + (n-5)\sin(\pi/3)\cos(3\pi/4)$$

$$\xi_2^{(n)} = 10 + (n-5)\sin(\pi/3)\sin(3\pi/4)$$

$$\xi_3^{(n)} = (n-5)\cos(\pi/3) \ , \quad n = 1, \ ---20$$

A tentative origin 0 in the neighborhood of the crack is taken at (0.2, 0.3, 0.15). The inversion integral then leads to a number of layers for given source and observation points as described earlier. For a source at S_k and an observation point at Q_n the pair of layer-end-planes $\Omega(k,n;p)$, p = 1,2 obtained from Eq. (40) are defined by

$$q_1(k,n)\,\xi_1 + q_2(k,n)\,\xi_2 = \pm \{a^2 q_1^2(k,n) + b^2 q_2^2(k,n)\}^{1/2} \qquad (43)$$

where $\pm$ signs correspond to p = 1,2, respectively. The bisector vector $\underline{q}(k,n)$ is associated with $\overline{OS}_k$ and $\overline{OQ}_n$.

For large n, each set of planes $\Omega(k,n;p)$ defined by Eq. (43) for a given k, forms a prismatic surface, which will touch the crack-edge C at a set of points. These points span a polygon, which approximates a segment C(k;p) of the edge C. The intersection of the two prismatic surfaces for the same p but k = 1 and k = 2, respectively, will lead to points on C common to C(1;p) and C(2;p). We can use these points to generate the crack-plane. The above points are obtained as follows. The prismatic surface formed by the first-set of planes $\Omega(1,n;p)$ will be intersected by the various individual planes of the set $\Omega(2,n;p)$ along a set of polygons $\Gamma(2,n;p)$, which we initially determine. The points where the polygons of this set intersect in 3-D space constitute points for an approximate determination of the crack-plane. These points are easily found by testing where any polygon $\Gamma(2,n;p)$ with a given n is intersected by the remaining planes of $\Omega(2,n;p)$. The plane of the crack can thus be determined, and once this has been achieved the

intersection of this plane with the set of planes $\Omega(k,n;p)$ gives the desired tangent lines enveloping the crack edge. For a = 1 and b = 0.5, Table 1 gives the vertices of the polygon formed by the tangent-lines corresponding to $\Omega(1,n;1)$ which envelopes the arc $C(1;p)$ with p = 1. These points evidently lie very close to the crack-plane $\xi_3 = 0$. The last column of Table 1 shows that these points lie very close to the elliptical boundary as well. A similar set of points corresponding to the arc $C(1;p)$ with p = 2 is also generated by the above calculations, since they define an opposite quadrant of the crack-edge referred to the origin at the center of the crack.

The extent of the crack-edge recovered will depend on the relative locations of S_k and Q_n with respect to the crack-plane. A proper choice can usually be made once the crack-plane is determined from an initial configuration.

ξ_1	ξ_2	ξ_3	$\xi_1^2/a^2 + \xi_2^2/b^2 - 1$
.85076	.26265	.00041	-.26033E-03
.82938	.27927	.00036	-.16001E-03
.80476	.29679	.00031	-.40334E-04
.77657	.31505	.00026	.10016E-03
.74455	.33388	.00020	.26192E-03
.70851	.35301	.00014	.44407E-03
.66841	.37211	.00007	.64425E-03
.62437	.39084	.00000	.85866E-03
.57670	.40881	-.00007	.10824E-02
.52589	.42566	-.00014	.13099E-02
.47260	.44107	-.00022	.15359E-02
.41760	.45480	-.00029	.17556E-02
.36175	.46667	-.00036	.19654E-02
.30585	.47661	-.00043	.21628E-02
.25070	.48464	-.00049	.23466E-02
.19695	.49085	-.00055	.25162E-02
.14513	.49538	-.00061	.26719E-02
.09565	.49841	-.00066	.28143E-02
.04877	.50014	-.00071	.29440E-02

Table 1: Computed coordinates of vertices of polygon enveloping the crack edge, for a = 1 and b = 0.5. Coordinates relative to origin at center of elliptical crack.

ACKNOWLEDGEMENT

This paper was sponsored by the Center for Advanced NDE operated by the Science Center, Rockwell International, for the Advanced Research Projects Agency and the Air Force Materials Laboratory under Contract F33615-74-C-5180. The assistance of A. K. Gautesen and H. McMaken (direct problem) and K. Viswanathan and A. Norris (inverse problem) is gratefully acknowledged.

REFERENCES

1. Achenbach, J. D., Gautesen, A. K., and McMaken, H., "Application of Geometrical Diffraction Theory to QNDE Analysis," in Proceedings of the ARPA/AFML Review of Progress in Quantitative NDE, 1978 (edited by D. O. Thompson), Science Center, Rockwell International, Thousand Oaks, Cal., January 1979, pp. 321-330.

2. Achenbach, J. D., Gautesen, A. K., and McMaken, H., "Diffraction of Elastic Waves by Cracks - Analytical Results," in Elastic Waves and Non-Destructive Testing of Materials (edited by Y. H. Pao), American Society of Mechanical Engineers, AMD-29, 1978, pp. 33-52.

3. Cohen, J. K., Bleistein, N. and Elsley, R. K., "Nondestructive Detection of Voids by High-Frequency Inversion Technique," in Proceedings of the ARPA-AFML Review of Progress in Quantitative NDE, 1978 (edited by D. O. Thompson), Science Center, Rockwell International, Thousand Oaks, Cal., January 1979, pp. 454-458.

4. Cohen, J. K. and Bleistein, N., "The Singular Function of a Surface and Physical Optics Inverse Scattering," WAVE MOTION 1, 1979, pp. 153-162.

5. Achenbach, J. D., Viswanathan, K. and Norris, A., "An Inversion Integral for Crack-Scattering Data," WAVE MOTION 1, 1979, in press.

6. Achenbach, J. D., and Gautesen, A. K., "Geometrical Theory of Diffraction for Three-D Elastodynamics," J. Acoust. Soc. Amer., 61, 1977, pp. 413-421.

7. Gautesen, A. K., Achenbach, J. D., and McMaken, H., "Surface-Wave Rays in Elastodynamic Diffraction by Cracks," J. Acoust. Soc. Amer., 63, 1978, pp. 1824-1831.

8. Adler, L. and Lewis, K., "Frequency Dependence of Ultrasonic Wave Scattering from Cracks," in Proceedings of the ARPA/AFML Review of Progress in Quantitative NDE, 1978, (edited by D. O. Thompson), Science Center, Rockwell International, Thousand, Oaks, Cal., January 1979, pp. 393-399.

9. Achenbach, J. D., Adler, L., Lewis, D. Kent, and McMaken, H., "Diffraction of Ultrasonic Waves by Penny-Shaped Cracks in Metals: Theory and Experiment," J. Acoust. Soc. Amer., in press.

10. Gautesen, A. K., "On Matched Asymptotic Expansion for Two-Dimensional Elastodynamic Diffraction by Cracks," WAVE MOTION 1, 1979, pp. 127-140.

11. Adler, L. and Lewis, D. K., "Diffraction of Ultrasonic Waves by Elliptical Cracks in Metals," this volume.

12. Whalen, M. F., O'Brien, L. J., Mucciardi, A. N., "Application of Adaptive Learning Networks to Determine Size and Orientation of Two-Dimensional Flaws in Solids," this volume.

13. Achenbach, J. D., Norris, A., and Viswanathan, K., "Inversion of Crack-Scattering Data in the High-Frequency Domain," Recent Developments in Classical Wave Scattering: Focus on the T-Matrix Approach, Pergamon Press, 1980.

SUMMARY DISCUSSION
(J. D. Achenbach)

Unidentified Speaker: I wasn't quite sure on that one plot that you put on and took off, where there were experimental points. Is that the same thing as Bernie talked about last year? Is Bernie here? Is that the same kind of plot you showed last year? Is that the comparison between your theory and Laszlo's experiments?

J. Achenbach: Okay. I will show you that one. Laszlo will talk about similar things, but here is plotted the relative amplitude versus the frequency. At three, four locations. The angle of observation is at 35, 45 degrees, 55 degrees, 60 degrees. It compares theoretical results which were obtained on the basis of these ray theory considerations which I pointed out, and then the dots are the points that Laszlo measured. So he has gone up to 14 megahertz. The point I was trying to make with this plot is that it is important for the inverse method to know something about the spacing of the peaks because the peaks come about because of the interference of rays. The interference of the rays is related to the dimension of the crack. So, if I can get this spacing of the peaks reasonably accurately, I am in relatively good shape. I can't get the magnitude right for two reasons. The specimen is immersed in a water bath. The transition from the solid to the water we only approximately describe. There is a certain damping effect there. And the titanium has a certain amount of damping. Perhaps the water also. So, it's natural that at a higher frequency the agreement becomes worse because of damping.

Unifentified Speaker: The other question was: in your equation for the C.O.D., how do you devise change in the C.O.D.? Do you make C.O.D. measurements?

J. Achenbach: No. These are computed.

Unidentified Speaker: Laszlo will talk --

J. Achenbach: Laszlo is not involved in this work. This is a different theory. What we did was, we said we can either use ray theory all the way out in the field away from the crack and then we get conceivably into trouble at shadow boundaries. And that is just because of the asymptotic nature of the theory. An alternative would be just to use ray theory to compute the crack opening displacement. In other words, the fields on the crack faces. And then stick that result into this elastodynamic representation theorem, and then things integrate nicely out, and you get the field everywhere bounded. You get it bounded at shadow boundaries, you get it bounded at caustics - and that's the idea of introducing the crack opening displacement.

Jim Krumhansl (Cornell University): Could I just add: the point about this, of course, is that in a certain sense the method exhibits some of the properties that one could have gotten from acoustics, simply a scaled approximation, but now you can pick out a particular type of incident wave and you can compare the features of the longitudinal to the transverse wave, and elastodynamics allows you to get some semi-quantitative, fairly quantitative, measure of the magnitude of the relative features in those different polarizations.

J. Achenbach: That's right. Of course, the elastodynamics appears when the coupling between longitudinal and shear waves is built in, because it's built in, in the way the signals distribute over those two cones. If I had pure acoustics, I would only have one cone. If I had treated this problem as a pure acoustic problem, the longitudinal wave diffracted by an edge would produce just a diffracted longitudinal wave. Here it produces both. However, we never use those transverse waves because, I guess, in experiments you only work with the first arrival anyway. As soon as you can measure transverse signals, then we will stick in these other transverse signals, and you get the whole field.

Jim Rice (Brown University): Just for clarification, the inversion procedure is based on extremely high frequencies in that limited crack face is motion taken into account?

J. Achenbach: If you can follow my hands here from the two crack tips, at low frequency you would have an ellipse. At high frequency you have waves on the crack faces; at still higher frequencies you have more waves. We ignore the wiggles due to secondary surface motions.

(continued)

J. Achenbach (discussion continued)

Jim Rice: When you compare your inversion procedure with experiments, how small must the wavelength in fact be compared to crack size for this kind of an approximation?

J. Achenbach: Okay. We have to let Laszlo discuss this; he will show that in the next talk because we used physical elastodynamics for an elliptical crack. You can actually work out analytically the results, and you get a Bessel function and compare it with experiments. The comparison was good for a wavelength range which he will show.

# #